INTERNATIONAL ATOMIC ENERGY AGENCY
UNITED NATIONS EDUCATIONAL, SCIENTIFIC AND CULTURAL ORGANIZATION

INTERNATIONAL CENTRE FOR THEORETICAL PHYSICS
34100 TRIESTE (ITALY) - P.O.B. 586 - MIRAMARE - STRADA COSTIERA 11 - TELEPHONES: 224281/2/3/4/5/6
CABLE: CENTRATOM - TELEX 460392-1

SMR/107 - 26

WORKSHOP ON PATTERN RECOGNITION AND ANALYSIS OF SEISMICITY

(5 - 16 December 1983)

NEW STATISTICS OF SEISMICITY RELEVANT TO PREDICTION STUDIES

A.G. Prozorov

A.G.Prozorov

New statistics of seismicity relevant to prediction studies

We shall consider in this lecture a few statistical properties of space-time distribution of earthquakes, which has not yet come to the level of application of the pattern recognition technique. There will be discussed three types of properties:

(i) anomalies of space distributions of statistics of seismicity such as swarming rate, average depth of foci, creepex etc.;

(ii) significant time variations of the properties of seismicity in the vicinity of strong earthquakes - local statistics;

(iii) large scale time-space changes of seismic regime.

I. Space distribution anomalies (on the example of Mexican region) [1].

The traditional statistic - $N(x)$ - is the number of events in a earthquake catalog in a unit of space and time with the centre in a poin x.

Distribution of N is poissonian

$$P\{N = k\} = \frac{\lambda^k}{k!} e^{-\lambda},$$

where λ is the intensity of the flow of seismic events, on the condition that earthquakes in the catalog are independent of each other and intensity λ is constant in space and time.

If we take as a unit of time the whole period of observations the statistic N will be close to the map of epicentres (Fig. I). The notation on the Figure is as follows: one event is denoted by a dot, 2 and 3 by open triangle, 4 and 5 by an open square, 6 to 10 by a filled triangle and more than 10 by a filled square.

It is evident from the Figure that $\lambda = \lambda(x) \neq$ const. The distribution shows main features of the tectonics of the region: continuation of San Andreas fault system, Pacific ocean ridges and fracture zones, subduction zone along the Pacific coast of Central America.

Space distribution of seismicity is not fully described by the distribution of epicentres especially in the subduction zones. The traditional way to study such zones is two-dimensional cross-sections of zones along some straight lines on the surface of the region. This approach is usefull but does not give the whole three-dimensional picture. Some details of the Benioff zone structure can escape from attention.

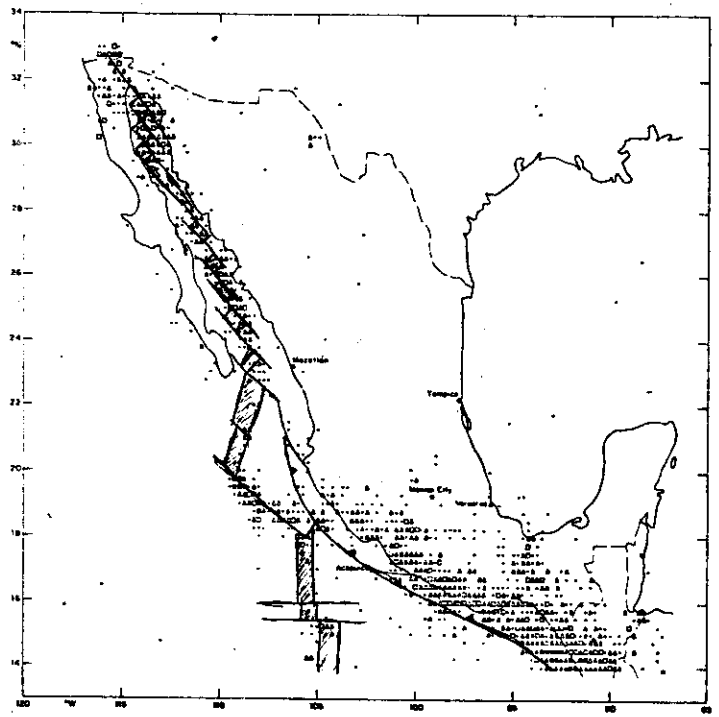

Figure 1. Distribution of number of earthquakes in the Mexico region. One event is denoted by a dot, 2 and 3 by an open triangle, 4 and 5 by an open square, 6 to 10 by a filled triangle and more than 10 by a filled square.

The statistic of average depth of foci in a given volume of the region with the centre in point x - $h_{av}(x)$ - provide good supplement to the cross-section method (Fig. 2).

The notation on Figure 2 and following ones is adjusted to the actual distribution of the statistic on two dimensional grid of points. The si of the grid is 0.5^{o} in latitude and longitude. Filled symbols denote values of the statistic above the average, calculated for the total sample of grid points; open symbols denote values below the average. Circles represent values from the average up (down) to 0.5 , triangle to I,0 , diamond to I.5 and encircled diamond above (below) I.5 , where is the squre root of variance.

Increase of average depth in SW-NE direction in the area to the east of 96^{o}W shows the well established direction of Benioff zone in the orthogonal direction (SE-NW), which correlates perfectly with volcanism line on the deep edge of the zone. The increase of $h_{av}(x)$ in S-N direction in the area to the west of 96^{o}W reveals new direction (W-E) of Benioff zone in this area. This part of Benioff zone is also correlated with volcanoes line (especially recent ones) which include famous Apocatepetl and Popocatepetl beside Mexico.

To satisfy the condition of constant λ and have Poissonian distribution of N the statistic N is usually considered for fixed volume of seismic region V, very often for the whole region: $N_{\Delta T}$ is the number of events in the area V in a unit of time. Variations of seismicity in time are not so large as in space. Still there are significant fluctuations especially during the swarms of aftershocks after some earthquakes.

To avoid distortions caused by swarms of aftershocks it is necessary to separate main events in the catalog and their aftershocks [2]. There are many algorithms to do that, one of them has been studied here in the school.

Fig. 3 shows distribution of the number of main events in the catalog - $N_{m}(x)$. The level of seismicity on this histogram is considerably reduced in the North of the Gulf of California, off-shore of Jalisco and around Pinotepa Nacional (98^{o}W - 16^{o}N). Notation here is the same as in Fig. I.

The statistic of $N_{m}(x)$ gives the most unbiased picture of seismic activity and it should be used as essential part in the algorithm of earthquake hazard estimation.

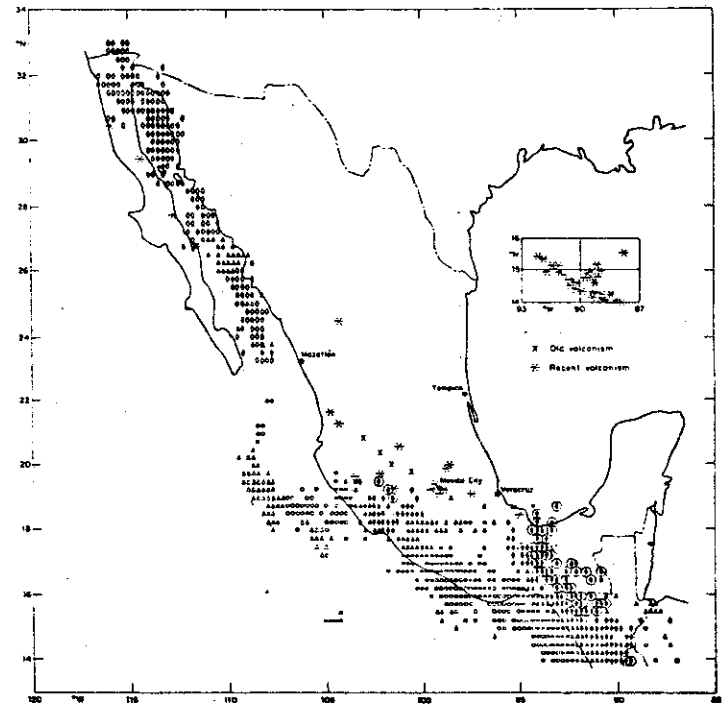

Figure 2. Average focal depth distribution. Filled symbols denote values of the statistic above the average, calculated for the total sample of grid points; open symbols denote values below the average. Circles represent values from the average up (down) to 0.5 σ , triangle to I.0 σ , diamond to I.5 σ and encircled diamond above (below) I.5 σ , where σ is the square root of variance.

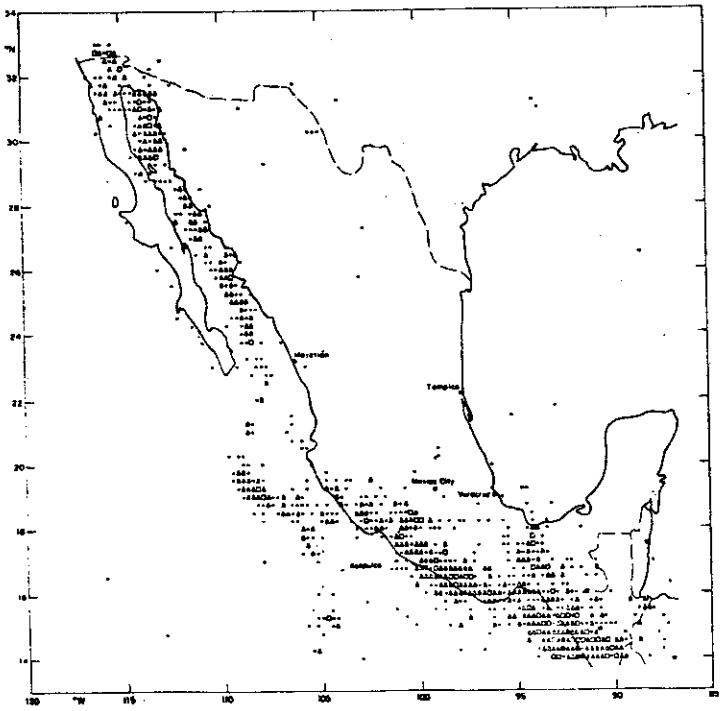

Figure 4. Distribution of main events in the Mexico region (aftershocks excluded). Notation as in Figure 1.

Aftershocks separeted from main events are also of interest for the study of seismic regime. The statistic of positive influence of main events or swarming rate is defined as an average number of aftershocks created by main event of magnitude M in a unit interval ΔM of magnitude $(M-\Delta M, M)$. Positive influence is estimated via the total amount of aftershocs $n_a(M_o, M+\Delta M)$, where M_o is the lower limit of magnitudes in the catalog, M is the magnitude of main shock, and ΔM is elementary subinterval of magnitudes (=0.5) from which main events are taken, as follows [2]

$$p = \frac{n_a}{\alpha(M)} ,$$

where $\alpha(M)$ is defined by recurrence time law as it is shown on the Fig. 4. Coefficients $\alpha(M)$ for Mexico region are shown on table I.

It turns out that this characteristic is almost independent of M . It supports the hypothesis about automodel type of seismicity in a wide range of their energies.

Positive influence p(x) (Fig. 5) is high in mid-ocean ridges and in places with thick sediment layers as in the delta of Colorado river and off-shore of Mexico-Guatemala border. The last cause of high positive influence was first discovered in the Central Asia in 1972.[3] Physical explanation of that can be attributed to the Mogi experiments with samples of rocks. They show higher swarming rate for soft, heterogeneous materials comparatively to strong and consolidated ones.

Positive influence value is an important characteristic of the type of seismicity in the region. In regions with high p-values there are many swarms, strong earthquakes are rare and they usually preceeded by a prominent groups of foreshocks which make easier their prediction. Low p-values areas with the same level of seismic activity are generally more dangerous because strong earthquakes are relatively more often and quite often are not preceeded by foreshocks at all.

The global distribution of positive influence is shown on Fig. 6. The notation here is different from Mexican maps. The scale is logarithmic, digits 9 to I correspond to the following number of aftershocks: 9 to 100; 8 to 63; 7 to 40; 6 to 25; 5 to 16; 4 to 10; 3 to 6.2; 2 to 4.0; I to less than 2.3 aftershocks per standart main event and dot corresponds to a cell which has non-zero number of main events but no aftershocks.

Table 1.

Correction factor $\alpha(M)$ for the positive influence calculation in the Mexico region, $\Delta M = 0.5$.

M	4.0-4.4	4.5-4.9	5.0-5.4	5.5-5.9	6.0-6.4	6.5-6.9	7.0
$\alpha(M)$	1.0	2.084	6.687	25.376	77.129	160.4	241.6

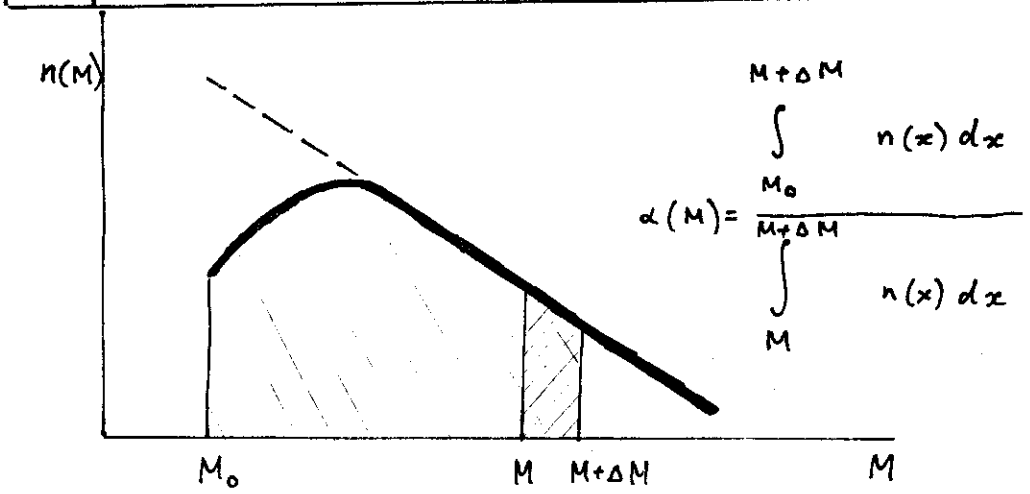

Fig. 4

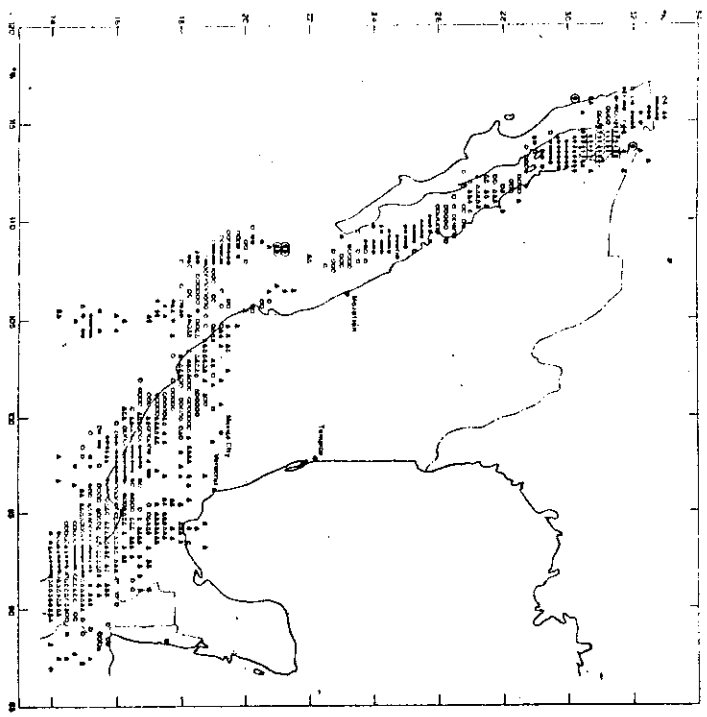

Figure 5. Positive influence (swarming) distribution. See text for definition. Notation as in Figure 2

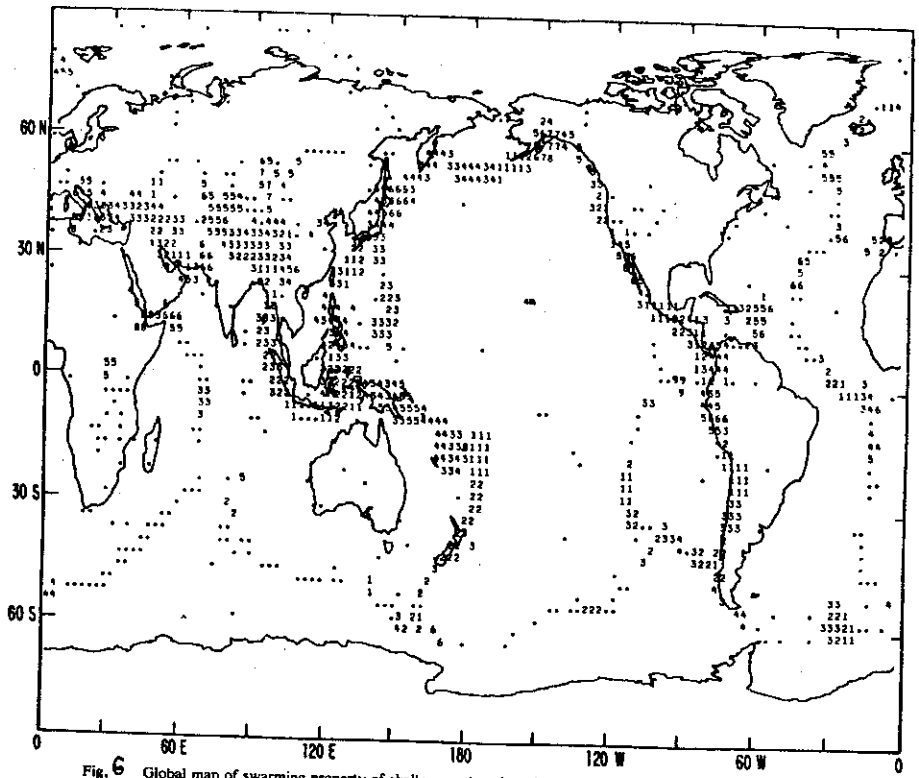

Fig. 6 Global map of swarming property of shallow earthquakes. The scale is logarithmic, as stated in equation (27); if in an area with a maximum swarming value of 9 an earthquake produces 100 aftershocks, index 8 corresponds to 63 aftershocks, 7 to 40, 6 to 25, 5 to 16, 4 to 10, 3 to 6.2, 2 to 4.0, and index 1 represents less than 2.3 aftershocks per standard event. Dots designate areas in which initial events had no detected ($m_b \geq 5$) aftershocks.

There are considerable changes of positive influence on the world map. The largest values are situated in the Colorado Delta, but very near it, in the Central California the swarming is low.

High contrasts of positive influence are situated in South America: low p-values between 15°s and 25°s are neighbouring with areas of high p-values to the North and to the South of this area.

On the western part of the circum-Pacific belt high swarming values are situated in Hokkaido and Kuril islands, in the Philippines, New Guinea and New Hebrides.

There is some consistent behavior of swarming in other areas. On mid-oceanic ridges there are bursts of swarming usually near triple junctions and major fracture zones, for example, the triple junction near Bouvet Island in the South Atlantic, the Southern part of the Red sea and the Gulf of Aden, the Challenger fracture zone in the Pacific and the Romanche and Gibbs fracture zones in the Mid-Atlantic Ridge.

The complicate pattern in the Alpine belt needs a more detailed study.

It is interesting to compare variations of positive influence with depth of foci of the main shocks. In Soviet Central Asia it has minimal values in depth range 120 - 160 km which corresponds to the low velocity layer in this region (Fig. 7)[3].

Possible physical interpretation of it may be in high viscocity of the material in low velocity layer which dissolve effectively additional stresses applied by the main earthquakes to adjacent areas.

Variations of p(h) on the global scale are shown in Table 2[2]. Zone from 250 to 450 km of intermediate main shocks appear to have no detectable aftershocks. Interpretation of this fact is unknown.

Now let us come to the study of magnitude distributions. It is well known that the distribution is linear in semilogarithmic scale

$$\log P(M) = A - b\,M\,, \quad M \geq M_o\,.$$

The maximum likelihood estimation of b is

$$b = \frac{\log_{10} e}{M_{av} - M_o}$$

where M_{av} is the average magnitude in a sample.

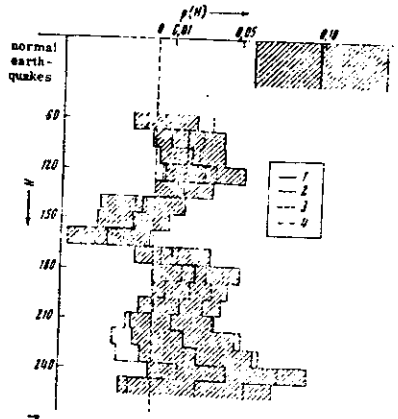

Fig. 7. Evaluation of the effect p of the initial earthquakes upon subsequent earthquakes in the time interval $\tau \leq 15$ days and the distance interval $d \leq 15$ km. Earthquakes intensity: group V in 1952 to 1956, and k = 9 to 12 in 1957 to 1961. The initial earthquakes occurred in the depth interval $\Delta H = 30$ km; the sliding step interval is 10 km. 1 - evaluation of p; 2 - 90% confidence level for p; 3,4 - evaluation of p from the 1952-1956 and 1957-1961 data, respectively.

TABLE 2 Dependence of Positive Influence $p(h)$ on Depth of Focus of Initial Earthquakes

Depth Range, km	Number of Initial Earthquakes	Total Number of Aftershocks	$p(h)$	Standard Deviation
100–150	801	13	0.005	0.001
150–200	357	8	0.006	0.002
200–250	173	3	0.006	0.003
250–300	50	0	0.	...
300–350	46	0	0.	...
350–400	48	0	0.	...
400–450	49	0	0.	...
450–500	46	3	0.030	0.017
500–550	82	2	0.005	0.003
550–600	147	5	0.012	0.005
600–650	97	10	0.022	0.007
650–700	10	0	0.	...

To study relation among strong and weak earthquakes in a sample we choose the statistic M_{av}. This statistic is robust in small samples and has physical meaning even in the case of non-linear recurrence time law. The last happened when it is used wide magnitude range in which reliably registered not all the earthquakes due to the losses by the network of seismic stations.

The next map shows the statistic of $M_{av}(x)$ (Fig. 8). High value anomalies are observed in Sierra Madre del Sur, near Petatlan (around 101°W and 17°N), in a spot off-shore of Jalisco and near the border of Guatemala and Honduras. A few patches are also seen in the Gulf of California.

A low value anomaly is situated off-shore of Jalisco in a sharp contrast with the high values nearby. The geophysical interpretation of these anomalies is unknown, but it is evident that they can not be explained by the maximum magnitude distribution or by the inadequacy of the seismic network. The maximum magnitude distribution will be studied later on. For example, the high value anomaly near Petatlan could be attributed to the high maximum magnitudes observed in this area. However, the maximum magnitude around Pinotepa Nacional is about the same but the average magnitude is very low. The encircled filled diamonds off-shore of Jalisco on the average magnitude map can not be related to the inadequacy of the network for weak events, because further away from the shore a place is found with the opposite anomaly.

The next statistic creepex c(x) has been introduced using the experience in seismic source discrimination problem [8]. The main method of discrimination is the difference in surface and body wave generation by the earthquakes and explosions. The first class of events has in general larger size of source and smaller velocity of the development of the rupture than the second one. Roughly speaking it provides better conditions for generation seismic waves in lower end of the spectrum specifically surfase waves than in higher end of the spectrum - body waves.

The creepex c for an earthquake with surface wave magnitude M_s (measured at period T = 20 sec) and body wave magnitude m_b (T = 1 sec) is defined as

$$c = M_s - k\, m_b + l$$

or in other words as the distance from the straight line of the orthogonal least square fit for the sample of events with M_s and m_b listed in a given catalog $M_s = k\, m_b - l$.

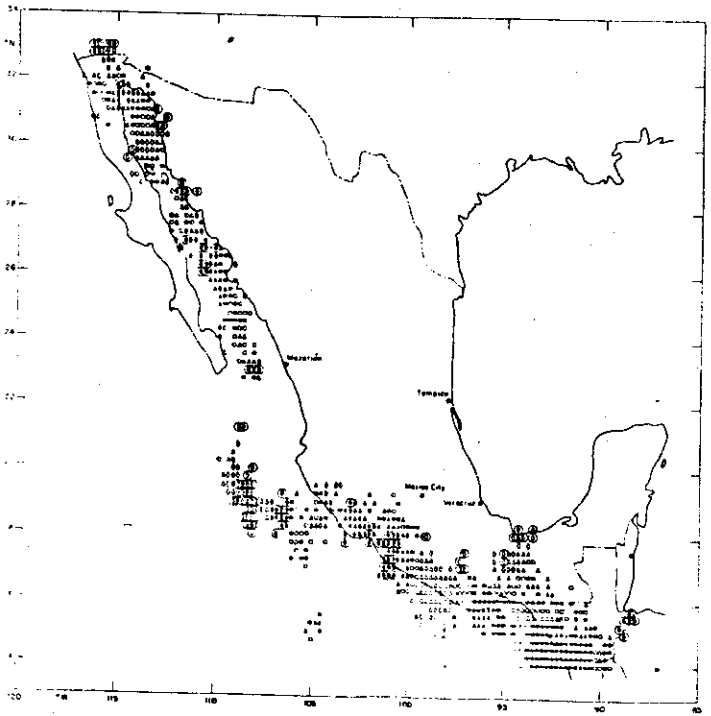

Figure 8. Map of average magnitude in the interval (M_o, M_{max}), M_o = 4.0. Filled symbols denote values of the statistic above the average, calculated for the total sample of grid points; open symbols denote values below the average. Circles represent values from the average up (down) to 0.5 σ, triangle to 1.0 σ, diamond to 1.5 σ and encircled diamond above (below) 1.5 σ, where σ is the square root of variance.

The coefficients for the global sample of the USGS catalog are k = 2.00 l = 5.34 (continuous line on the Fig. 9) and for Mexico region they are k = 2.68 and l = 8.58 (broken line).

A large value of c means that an earthquake generates more energy in the surface wave range (about 20 secs), a low value of c means that higher proportionof the energy released goes to the body wave range (about I sec). Creepex distinguishes earthquakes as a low frequency or a high frequency events. In other words, an earthquake can be thought as a "creepy" or an "explosive" type of event.

Fig. IO shows the creepex distribution in the Mexico region; notation is the same as in Fig. 2. The most prominent anomaly is high creepex values in the Pacific ocean ridges and fracture zones area. That can be explained by the the high heat flow or weakend materials in such areas which affect mainly going steep down body waves. Low creepex values are observed in the subduction zones of Sierra Madre del Sur and Sierra Madre. Creepex values are diminishing across the Benioff zone which could be due to the deepening of the sources and less effective surface wave generation. The steeper Benioff zone in Sierra Madre has lower creepex values than the Benioff zone of Sierra Madre del Sur.

The Northern part of Sierra Madre del Sur close to the Pacific ocean ridges and fractures zones has high creepex values as a continuation of creepex anomaly off-shore. In the Gulf of Tehuantepec, located between two subduction zones, creepex is high probably due to the Tehuantepec ridge.

In the Colorado River Delta region, creepex is very high which agrees with well known fact that the surface wave generation in this area is anomalously high comparatively to the neighbouring Peninsular Ranges region, where unfortunately we have data on creepex at all, probably due to low values of M_s which can not be detected by the WWSS network.

To the south of this area, in the Gulf of California, there is an alternate pattern of high and low creepex: high on ridges and low on transform faults.

The Mexico region contains three major tectonic structures: subduction zones, transform faults and ocean ridges and fracture zones. The highest values of creepex are observed on the ridges and fracture zones area; moderate ones in the transform faults in the Gulf of California and the lowest values in the subduction zones.

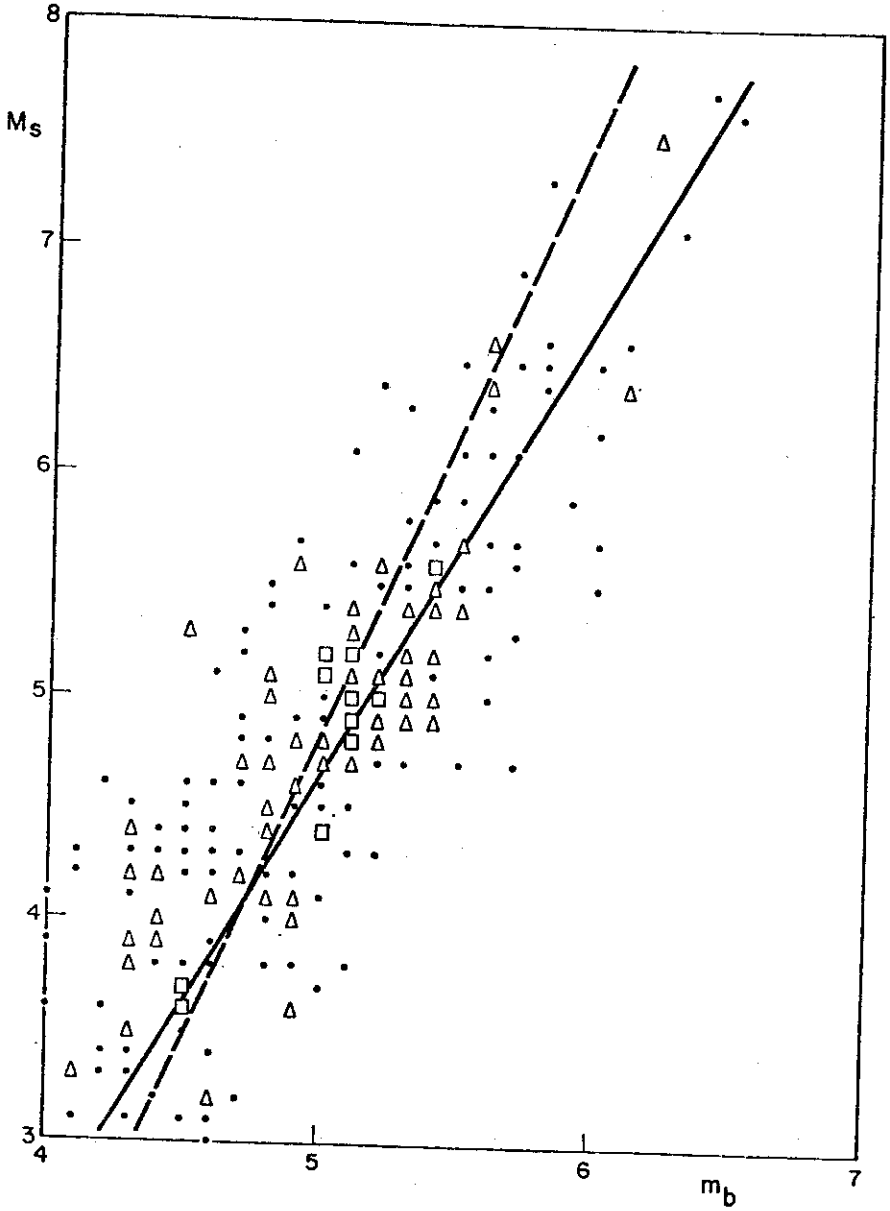

Figure 9. M_s vs m_b diagram for the Mexico region. One event is denoted by a dot, 2 and 3 by a triangle and 4 and 5 by a square. Broken line is the orthogonal least squares fit for the sample. Solid line is the same for the global sample not shown here.

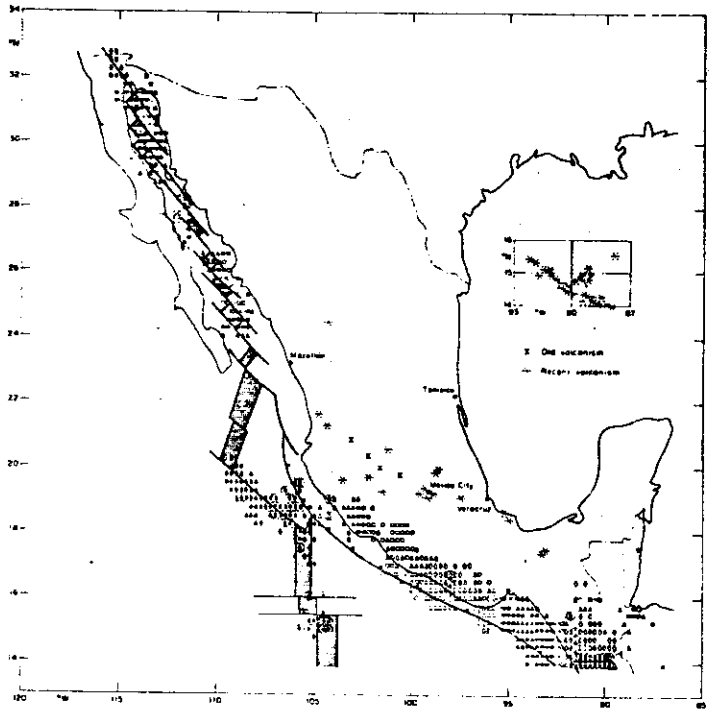

Figure IO. Distribution of the creepex in Mexico region.

On the global distribution of creepex the similar pattern can be seen (Fig.11). The notation here is as follows. The size of the grid is 2° in latitude and longitude. The distribution is smoothed in each direction (6°x6° cells are considered) but values are plotted in the central 2° x 2° cells which contain at least one seismic source. Values of c are indicated by open squares if $c < -0.3$; open triangles if $-.03 \leq c < -1.5$; open circles if $-1.5 \leq c < 0$; similar positive intervals of c are denoted by the corresponding filled symbols.

All the subduction zones: Japan - Kuril - Kamchatka, Sunda arc, South America and even isolated spot of subduction zone in Sandwich islands have low creepex values. New Hebrides, Fiji and Tonga - Kermadec area looks like exception, but in these regions two subduction zones collide, that can complicate the nature of the earthquake sources. Similar situation but of smaller scale is observed in the place of collision of two subduction zones in the vicinity of the Tehuantepec ridge.

On the other hand, high creepex values are seen almost everywhere along the mid-oceanic ridges especially in the triple junctions.

It is necessary, however, to notice that the interpretation of the creepex distribution can not be fully attributed to the explo-creep differences among sources of different regions. Considerable contribution in the fluctuations of c(x) from its average value is produced by the propagation effects from the sources of a given region to the whole network of seismic stations.

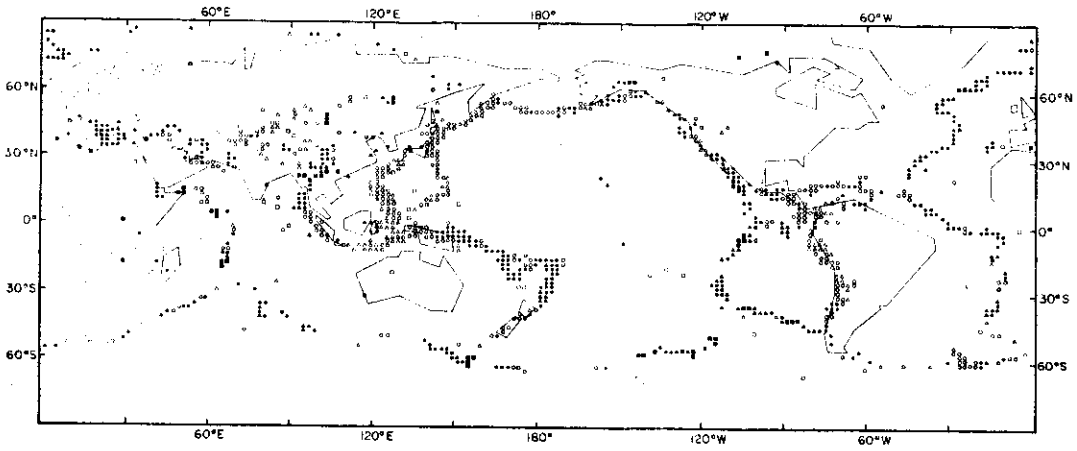

Figure II. Global distribution of creepex.

The next distribution of space properties of seismicity is the most important for the prediction problem - it is the distribution of maximal observed magnitude (Fig. I2). Notation here is as follows: a dot represent the maximum magnitude observed in a given grid point during the period I964 - 80 in the interval (4.0, 4.9), an open triangle corresponds to the interval (5.0,5.9), an open square to (6.0, 6.9) and a filled square to a magnitude greater or equal than 7.0 .

The largest number of 0.5°x0.5°-cells with magnitude greater or equal to 7.0 is observed on the south-west slopes of Sierra Madre del Sur; less numerous on the Sierra Madre and somewhat lower maximum magnitudes are observed in the Gulf of California and on the Pacific ocean ridges and fracture zones off-shore of Jalisco and Colima.

The place off-shore of Jalisco, which has high values anomaly on the main events seismicity map, produce, however, maximum observed magnitude below 6.0 . This fact draws attention to the complicate relations among the parameters of seismicity. They are rather independent. Table 3 shows correlation coefficients between them. Here the maximum observed magnitude is smoothed by using 0.75°x0.75° window and only cells with $M_{max} \geq 5.0$ are taken in the calculations. The threshold has been raised from $M \geq 4.0$ because we are interested in the behavior of the parameters in highly active zones. As for the other parameters the smoothing window of 1.75°x1.75° is used.

In order to provide a reasonable accuracy in the estimates of the parameters, the number of events in the smoothing window is restricted as follows: not less than 5 for creepex and positive influence; not less than 20 for average magnitude.

The correlation coefficients are not large in absolute value which confirms our previous conclusion that the parameters are rather independent.

Random variables at close grid points are not independent due to smoothing, so it is difficult to make a definite statement about statistical significance at the correlation coefficients. However, relatively large coefficients indicate some relations between the parameters.

Of course, creepex is negatively correlated with the average focal depth due to the lower efficiency of sources in surface wave generation when the depth of focus is larger. However, the average focal depth does not explain the whole picture of creepex. For example, earthquakes in the Gulf of California are shallower than in the Pacific Ocean ridges and fracture zones area, but the creepex is much higher in the latter area. Creepex in general is lower in the Sierra Madre del Sur and the Sierra Madre areas which agrees with high values of average focal depth here. But the Tehuantepec ridge anomaly of

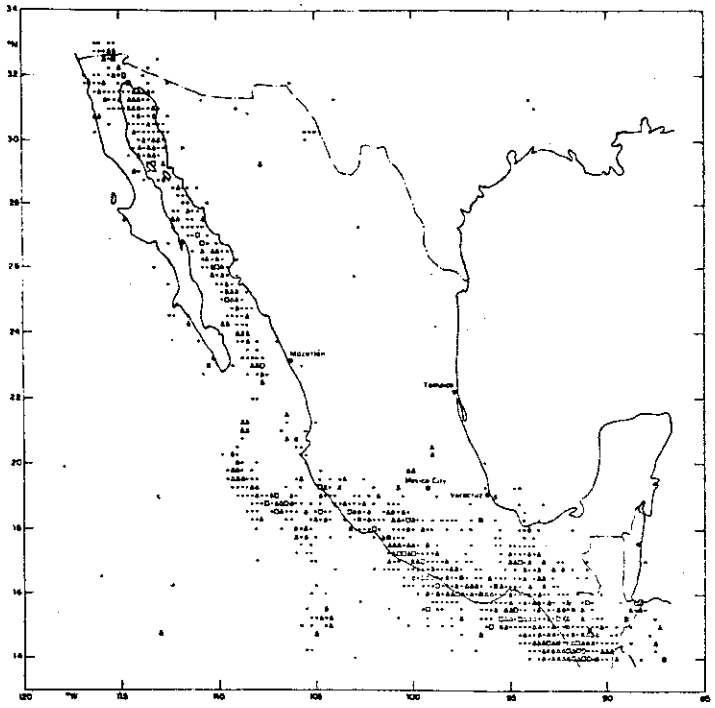

Figure I2. Map of the maximum magnitude observed during the period 1964-1980. A dot represents maximum magnitude in the interval (4.0, 4.9), an open triangle in (5.0, 5.9), an open square in (6.0, 6.9) and a filled square a magnitude greater or equal than 7.0.

Table 3

Correlation between the parameters of seismicity: maximum observed magnitude $M_{max}(\vec{x})$, main events seismicity $N_m(\vec{x})$, average magnitude $M_{av}(\vec{x})$, average focal depth $h(\vec{x})$, cree-pex $c(\vec{x})$ and positive influence $p(\vec{x})$.

Parameter	Number of active grid points.	Average value a and r.m.s. fluctuation σ of the estimates for: first parameter				Correlation coefficient.
				second parameter		
first second	n	a_1	σ_1	a_2	σ_2	r
M_{max} N_m	733	5.85	0.67	60.83	41.99	0.21
M_{max} M_{av}	692	5.88	0.68	4.65	0.09	0.25
M_{max} c	534	5.95	0.68	0.14	0.26	-0.08
M_{max} p	728	5.86	0.68	0.05	0.08	-0.11
N_m M_{av}	773	60.76	40.26	4.64	0.09	0.01
N_m c	563	66.80	43.40	0.14	0.26	-0.34
N_m p	854	55.95	41.09	0.05	0.08	0.04
M_{av} c	566	4.65	0.09	0.14	0.25	-0.04
M_{av} p	773	4.64	0.09	0.05	0.08	-0.05
c p	583	0.14	0.26	0.06	0.09	0.08
p h	802	0.05	0.08	55.65	35.05	-0.43
c h	569	0.13	0.25	50.61	28.99	-0.40

creepex is not seen in the average focal distribution. Low creepex is associated with larger average and maximal observed magnitude and high main events seismicity, which is not surprising because of low creepex, beeng a quality of explosive earthquakes, shows places of either high stress in the area or high strength of the rocks or both.

Positive influence behave in a similar way to creepex relatively to average and maximal observed magnitudes but, of course, by its nature it can not be in negative correlation with main events seismicity.

Creepex and positive influence are positively correlated. Average magnitude and main events seismicity are positively correlated with maximum magnitudes, but these statistics are not independent from maximal observed magnitude by definition.

The last space distribution of the seismic property will be P-wave residuals.[7] The r.m.s. fluctuations of residuals are usually about I - I.5 secs and 95% confidence limit is about ± 3 secs. The distribution of residuals is confined to approximately ± 5 secs, and larger residuals are very likely due to significant errors in the determination of their arrival time. We do not include them in our calculations.

The r.m.s. fluctuations do not strongly depend on the quality of the stations; therefore for efficient stations which report to the ISC thousands of seismic events and for stations which report merely tens of events, the r.m.s. fluctuations are about the same. The similarity in r.m.s. fluctuations of residuals among stations suggests that a substantional amount of the fluctuations are not of station origin, but reflect errors in determination of the hypocentres due to regional and temporal variations in the travel times of the real earth compared to the constant tables. The averaging of residuals at a given station permit to cancel random fluctuations due to errors of different kinds. The standart deviation of mean residuals is as small as ± 0.I sec if stations are used which have reported I000 or more observations of P-wave arrivals.

Fig. I3 shows the geographic distribution of mean residuals for stations in North America. The distribution of residuals appears to be non-random with two major domains: there are positive residuals in the western part of the continent and negative residuals in the central and north-eastern part of the continent. The pattern is in good agreement with contour map of mean station corrections for the United States made by Herrin and Taggart, BSSA, 58, I968. The absolute

Figure I3. Distribution of P-wave travel time residuals in North America (in tenths of seconds).

Figure I4. Distribution of P-wave travel time residuals in Europe (in tenths of seconds).

values of the residuals are of the same order as given by Herrin and Taggart, although they determined them with different time tables. The spatial distribution is also in good agreement with the observations of Biswas and Knopoff, Geophys.J.R.astr.Soc., 36,1974., as well as with the magnitude anomalies in the USA observed by A.Douglas (personal communication) and with heat flow measurements (Simmons and Roy, 1969, AGU monograph 13).

Similarly the distribution of mean residuals in Europe seems to be non-random (Fig. 14). Most of the negative residuals are concentrated in northern Europe; positive residuals are spread over central Europe.

The large differences between positive and negative residuals in both Europe and North America are difficult to explain by local features beneath the stations, and they likely reflect lateral inhomogeneities in seismic velocities in the upper mantle.

II. Time variations of the properties of seismicity in the vicinity of strong earthquakes.

Detection of significant time variations of seismicity properties is generally more complicate comparatively to the study of space anomalies due to the reduction of the amount of data available for evaluation of the three-dimensional function instead of two-dimensional one.

To make some statistically significant conclusions let us concentrate our attention on the vicinities of strong earthquakes where the effect of preparation of them should be the strongest. That is what we call local statistics approach.

Another thing we can do to increase the statistical significance of the results is to neglect the differences in the process of preparation of single strong earthquakes and to study only features common for all of them. It allows us to join the samples of data available for all of them and consider it as the preparation of a one standard strong earthquake.

The followings are two properties studied in this way on the global scale.

Residuals of P-wave arrivals on 13 stations situated in 2°-vicinity of 4 earthquakes with $M \geq 7.5$ are displayed on the Fig. 15.[+] They are averaged in half year intervals (solid line); two thin lines shows the 95% confidence limits. Time equal to 0 corresponds to the time of strong events.

There is statistically significant rise of residuals 1.5 years before the strong earthquakes, it can be used for the prediction of the time of strong earthquake in the vicinity of seismic stations.

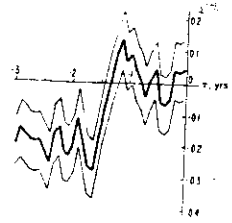

Figure 15

Half-year mean residuals (thick line) averaged on the thirteen stations situated in a 2° vicinity of four earthquakes with $M \geq 7.5$ which reported continuously to the ISC during three years before the earthquake occurrence. t is the time before the earthquake in years. The thin lines show 95% confidence limits for the mean values.

Another property is creepex which has been studied in the vicinities of 21 earthquakes with magnitudes $M \geq 7.5$.[4] The vicinities are as follows: 0°–1°; 1°–2°; 2°–4°; 4°–8° (Fig. 16, a – d). It has been also averaged in half year time intervals.

Fig. 16 d which refers to the distances range 4°– 8°, is essentially an eStimate of the behavior of $c(x,t)$ far away from major earthquakes. It shows a slight decline in the value of c in time which is to be expected due to the increase of the seismic network sencitivity.

However, there is a statistically significant drop in the c in the the half-year immediately preceding the earthquake origin time, which may reflect the build-up of tectonic strain in a broad area around the shock.

Fig. I a – c displays a behaviour quite different from the background pattern, although the beginning (positive) and end (negative) are essentially the same as in Fig. 16 d.

Differents in the patterns begin about four years before the main shock where a period of low c lasts untill one to one and a half years before the origin time. Again, this may be associated with the build-up of tectonic strain and stress.

Behavior of the creepex may be usefull in comparing different models of earthquake preparation. For example, in dilatancy-diffusion model decrease of creepex have to be associated with dilatancy phase, when cracks are open dry and consequently high frequent. After diffusion of the liquid from outside area which filled cracks again events became low frequent or creepex increase just before main shock.

In models of earthquake preparation without liquid as main feature of the process, like LNT developed in the Earth Physics Institute in Moscow, tectonic stress applied in the vicinity of future earthquake increase high part of the frequency content of background events (low creepex). Then dilatation phase lead to the opposite result in connection of creepex – opening the cracks and relative softening of the material (high creepex), and just before the main shock, background shocks concentrate in narrow area of future rapture zone, cracks in the outside area closed, material became more rigid again (low creepex).

Periods of low and high creepex are present on figures 16 a – c (although they not coincide exatly in time in different vicinities of the sources), but they are expected also in both types of models. The third phase of low creepex just before strong event (LNT-type models) is not found on fig. 16. However, in another time scale – Fig. 17 – where instead of time log t is taken low

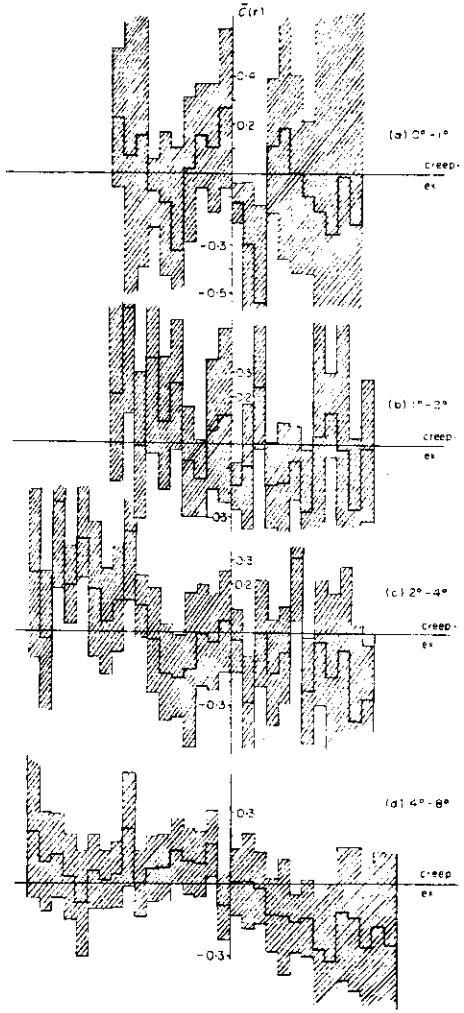

Figure 16 Behaviour of the creepex coefficient C in: (a) 0–1°, (b) 1°–2°, (c) 2°–4°, and (d) 4°–8° vicinities of 21 earthquakes with $M_{PS} \geq 7.5$. The time-scale is uniform in half-year intervals. The hatched region corresponds to 95 per cent confidence for random fluctuations about the average values.

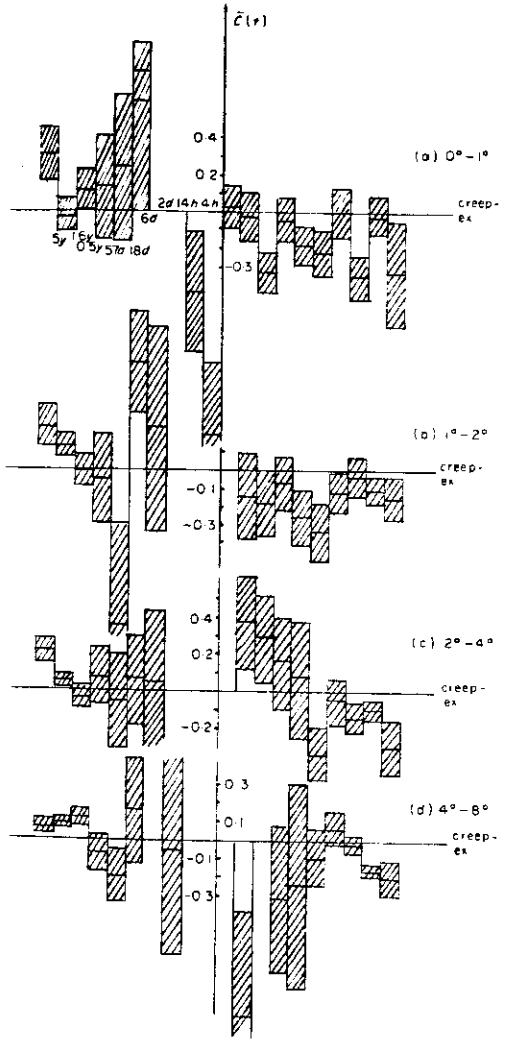

Figure 17 The same as Fig. 16 but with the time-scale in logarithmic intervals.

creepex values are observed a few hours before the main shocks.

To make independent test of the behavior of the creepex before strong earthquakes we select from the catalog events with magnitudes $6.5 \leq M < 7.5$, which are maximal in their 5°-vicinity during the period of observation (1968-1977). This procedure naturally exclude most active seismic regions. The sample contain about one hundred earthquakes from areas with moderate level of seismicity. Joining them into one sample similarly to the earthquakes with $M \geq 7.5$ we get similar pattern of behavior of c(t) - Fig. 18. All three phases are present, but time intervals of those phases are somewhat smaller, which is physically plausable due to smaller size of the earthquakes in the sample.

Let us consider now the changes of different properties of seismicity before strong earthquakes in a definite region - Mexico, Sierra Madre del Sur, earthquakes with magnitude $M \geq 7.0$. We consider average magnitude, creepex, maximum magnitude, main events seismicity, number of aftershocks and positive influence as a function of time in a 2°-vicinity of main events.

For computational convenience the distance between two points was calculated as the sum of the absolute values of differences in latitude and longitude. Smoothing time window is 5 months, elementary step is one month. The smoothing was carried out independently in two time intervals: 4 years before the main event and one year after. The major event was not included in either interval.

The vertical scale for each property is adjusted to the minimum and the maximum values of the parameters shown in each diagram in Fig. 19 and the whole interval is devided into 10 equal subintervals. The major event is not included in the maximum and minimum determination, but if their properties exceed these limits, they are plotted on the upper or lower ends of the vertical scale.

All the properties change considerably before the time of main events. Average magnitude, maximum magnitude and main events seismicity are low approximately from one to two years before the main events. That can be interpreted as a quiescence period, associated with the lock of tectonic movement. The hypothesis of lock of the movement and not simply lack of the movement is supported by a pronounced decline of creepex before this period of time.

The burst of positive influence 1.5 years before the main events may be explained by stress concentration in the region in this time interval.

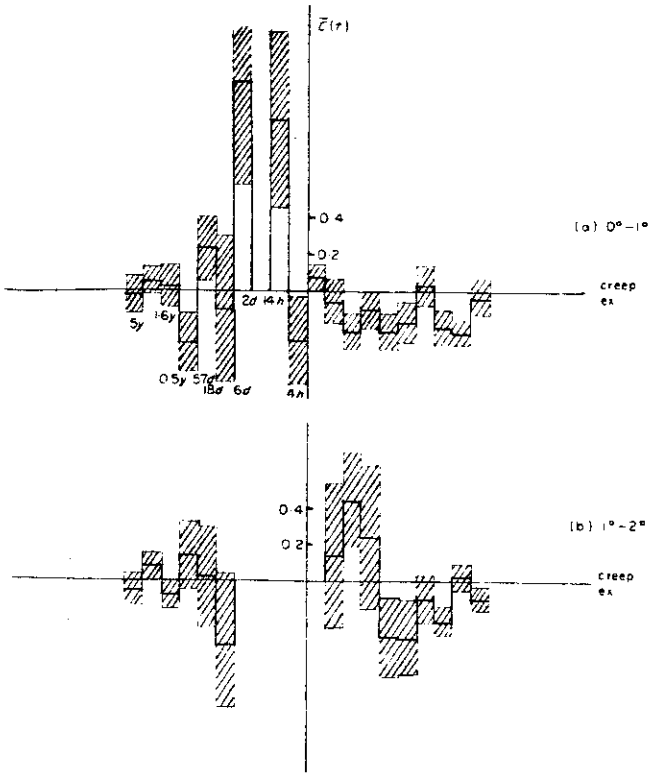

Figure 18. Information as in Fig. 17 for the vicinities of 100 earthquakes with $6.5 \leq M_{PS} < 7.5$ and which are maximum events in their ±5° vicinities (10° × 10° cells) during 1968–1977.

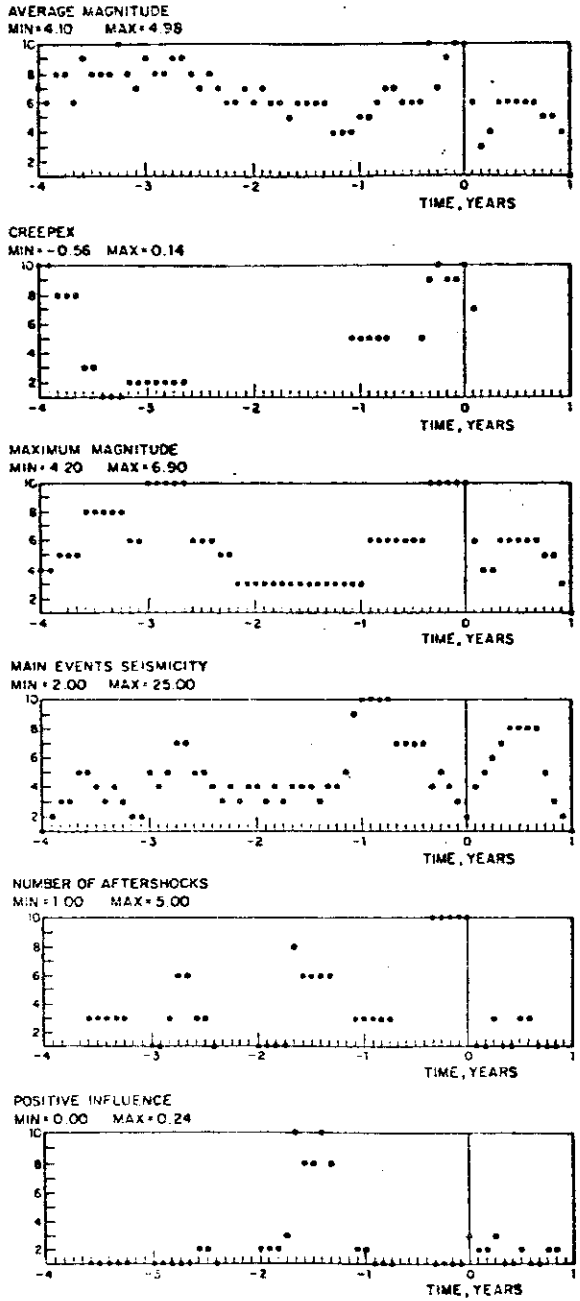

Fig 19.

Variations of the parameters of seismicity in 2 -degrees vicinity of earthquakes with M 7 in Sierra Madre del Sur area, Mexico region.

Later, during one year preceding the main events, rise of creepex indicates a phase of weakened material. It is accompanied by an increase of the average and maximum magnitude and a sudden rise followed by a decrease of main events seismicity.

III. Large scale time-space changes of seismic regime

This problem is even more difficult to study than local statistics. Again it is mainly due to the absence of adequate physical theory of tectonic processes which cause strong earthquakes. It leaves for seismologists the only way to search for empirical statistically significant features related to the preparation of strong earthquakes.

You have already thoroughly studied in the exercises course of the school one of such features. It is bursts of aftershocks preceding strong earthquakes in relatively large region size of which considerably excedes size of the rapture zone of earthquake.

The method has been successfully applied in a number of seismic regions of the Soviet Union and some other countries.

We shall only mention some other approaches. The hypothesis of seismic gap after major earthquakes which need long time for recovery to be able to produce another strong earthquake. It has been applied for prediction in Kuril - Kamchatka region in the Soviet Union and later in Japan, Alaska and other regions.

However, our recent results [10] show that aftershocks after moderate earthquakes follow the same recurrence time low as non-affected by initial earthquakes stress release. Strong earthquakes with magnitudes $M \geq 7$ shows slightly smaller probabilities of the aftershocks with big magnitudes than in completely random case. This fact seems to be in contradiction with the concept that the amount of energy after major earthquake is considerably reduced.

In the vicinity of earthquakes with $M \geq 8$ after the end of aftershock activity the intensity of seismic flow of events with $M \geq 7$ shows also very slight negative influence of initial shocks (decrease of intensity during the first 20 - 25 years of about 32% of average value) [13].

The exclusion of aftershocks, swarms and grouped events allows us to discuss the problem of changes of the intencity of seismic flow of large scale not related directly to the local disturbances.

Fig. 20 shows changes of the fraction Θ of Tyan-Shan region in the whole seismicity of the Soviet Central Asia. [3] The fraction Θ have been calculated in different periods of time in different magnitude ranges which were available at those periods. Size of rectangulars shows the 95% thresholds of random variations of the Θ. We can see that fraction Θ changes statistically significant

The scheme on Fig.20 is in agreement with the behavior of the absolute level of seismicity of Tyan-Shan region. The strongest earthquakes with magnitudes about 8 occured here at the turn of the XX-th century, and no earthquakes of this magnitude range were observed thereafter for for a long time. From 1939 there was no earthquakes with magnitude 7.

The increase of Θ in Tyan-Shan at the beginning of the century was accomplished by activization of a much larger size, namely of the eastern part of Soviet Central Asia and Himalayan region. 10 earthquakes with $M \geq 8$ were recorded in 60 years (1897 - 1956) in this area, but 7 of these events occured in 14 years (1897 - 1911). This is 95% significant in terms of Kolmogorov test.

Gutenberg and Richer noted a higher seismicity for the whole Earth during this period, which is 99% significant in terms of Kolmogorov's test applied to earthquakes with $M \geq 8$ taken from the catalog by Duda S.J. , Tectonophysics, v.2, No. 5, 1965.

Diagram on Fig. 20 shows that the intensity of seismic flow can change significantly in the time scale of years and tens of years and not only in geological times of tens of thousands and millions of years. Another important thing is that during evaluation of seismic danger one can make a mistake simply using extrapolation of the recurrence time law: the present activity of Tyan-Shan, for example, is 5 - 10 times lower than in other regions characterized by similar destructive earthquakes.

The existence of large scale stress field changes which are responcable for the statistically significant non-local changes of activity gives us an opportunity to try to locate them in time and space and use for earthquake prediction. This is the basis for the so called long range aftershocks. They have been found in Soviet Central Asia first [3] , in global scale [21] and with somewhat different time-magnitude thresholds in California [22].

The hypothesis is as follows: stress concentration applied to the region is detected via strong earthquake which the stress creates (A-event), it also provokes anomalously strong shocks (B-events) shortly afterwards in the asperities which are already in a critical condition for future strong earthquakes (C-events).

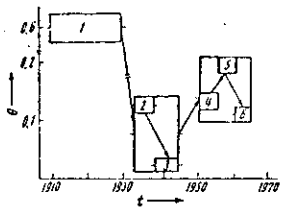

Fig. 20 The 95 percent significant changes in the fraction θ of seismicity in the northern Tien Shan' (region III of Fig. 2) as a function of the overall intensity of "migration" of earthquakes through the eastern part of Soviet Central Asia (evaluated by the binomial test [11]. The following energy ranges and time periods are involved: 1 - k ≥ 17, 1895-1911); 2, 3- intensity groups I-IV (2 - 1933-1938; 3 - 1940-1953; 4 - intensity group V, 1952-1956; 5, 6- k = = 9 - 12 (5 - 1957-1961; 6 - 1962-1965).

Fig. 2I shows B-events on the South California region created by all A-events befor e the time of each C-event in the region. A-events are not shown. We may see that all C-events are rather close to B-indicaters. B-events related to one C-event are removed from the map after the C-event occurence. Thresholds are as follows: $M_A = 6.0$; $M_B = 5.0$; $M_C = 6.4$; $T_{AB} = I$ year; $d_{AB} = 300$ km; $d_{BC} = I^{\circ}$.

To calculate statistical significance of the result we introduce function

$$A(x,t) = \begin{cases} \sum_{i=1}^{N} \frac{1}{2\pi\sigma^2} \frac{\theta_i(t)}{n(t)} e^{-\frac{|x-x_i|^2}{\sigma^2}}, & \text{if } n(t) \neq 0 \\ f(x), & \text{if } n(t) = 0 \end{cases}$$

where σ is the parameter of d_{BC}-accuracy of prediction; $f(x)$ is the seismic activity; $\int f(x)\,dx = I$; $n(t)$ is the number of B-events at the time t on the map of the region,

$$\theta_i(t) = \begin{cases} I & \text{, if } B_i \text{ is present on the map} \\ 0 & \text{, otherwise} \end{cases}$$

The domain $A(x,t)$ a is declared as "dangerous", where a is some parameter.

If we assume that strong earthquakes have the same density as small earthquakes and namely $f(x)$ and their occurences do not relate to B-events (0 - hypothesis), then the values of $A(x_c, t_c)$ will have distribution of probabilities $F(a) = P\{A(x_c,t_c) \leq a\}$

$$F(a) = 1 - \int_{T_1}^{T_2} \int_{G} \mathcal{D}(a,x,t) f(x)\,dx\,dt \qquad (*)$$

where

$$\mathcal{D}(a,x,t) = \begin{cases} 1, & \text{if } A(x,t) \geq a \\ 0, & \text{if } A(x,t) < a \end{cases}$$

We substitute as $f(x)$ in formula (*)

$$\hat{f}(x) = \frac{1}{K} \sum_{k=1}^{K} \delta(x - x_k)$$

where x_k are the coordinates of all earthquakes in the catalog without aftershocks.

Then using Monte-Carlo method we calculate $F(a)$ values for all C-events, they are shown in Table 4. With $\sigma = 40$ km the total level of confidence is 92.6%.

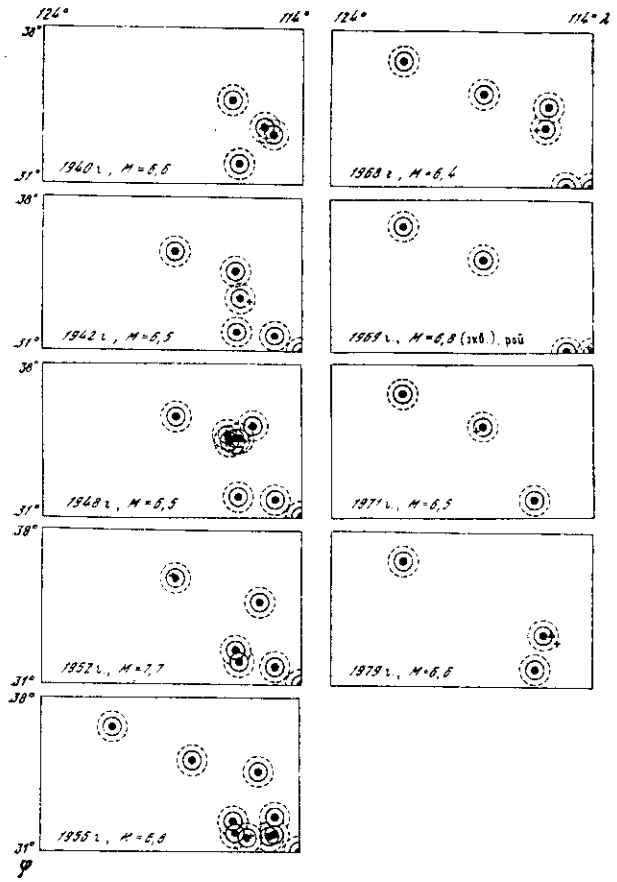

Figure 2I. Long range aftershocks in South California region.

Table 4. Significance levels of long range aftershocks in South California region.

N_C	M_C	$T=\infty$				T=10 лет	T=10 лет	T=15 лет	T=20 лет
		σ = 30 км	σ = 40 км	σ = 50 км	σ = 60 км	σ = 30 км	σ = 40 км		
1	6,6	95,9	98,8	99,2	99,4	96,1	98,0	98,1	98,3
2	6,5	89,5	88,9	87,7	86,5	91,1	91,6	90,7	90,3
3	6,5	97,0	98,4	99,0	99,2	98,2	98,5	98,3	98,3
4	7,7	96,9	96,2	94,8	92,8	94,0	91,5	93,0	93,7
5	6,8	91,5	91,6	93,4	96,4	93,4	93,5	92,7	92,2
6	6,4	93,0	92,6	91,7	91,1	90,8	88,9	89,8	90,5
7	5,8	89,8	91,0	91,9	93,7	83,0	77,8	82,1	84,1
8	6,5	96,7	96,7	96,1	95,4	90,3	86,9	89,3	90,9
9	6,9	78,8	79,4	78,9	78,5	78,7	78,7	78,5	79,1
10		92,1	92,6	92,5	92,5	90,6	89,5	90,3	90,8

Finally we shall consider Italian region studied during the school. Fig. 22 shows the preliminary results of search for long range aftershocks. Thresholds here were slightly changed comparatively to the South California. $M_A = 6.3$; $M_B = 5.0$; $M_C = 6.3$; $d_{BC} = 150$ km; d_{AB} without limitation inside the region; $T_{AB} = 2$ years; deep focus events ($h \leq 60$ km) have been used only as A-events.

All three events C after 1920 have B-events in their vicinity. Future alarms are concentrated in rather limited areas: Northern Apenines and Calabria arc. The latter is an area which experienced the strongest earthquake in this century in Italy (Messina, 1908, M = 7) and no strong earthquakes occured there since that time. Northern Apenines include the epicentre of the 1920 strong earthquake.

We would like to point out that information content of this map has rather limited practical importance and can not be used in practical warning of the people. However, B-indicated areas may get more attentive treatment in the future seismological studies of Italian region.

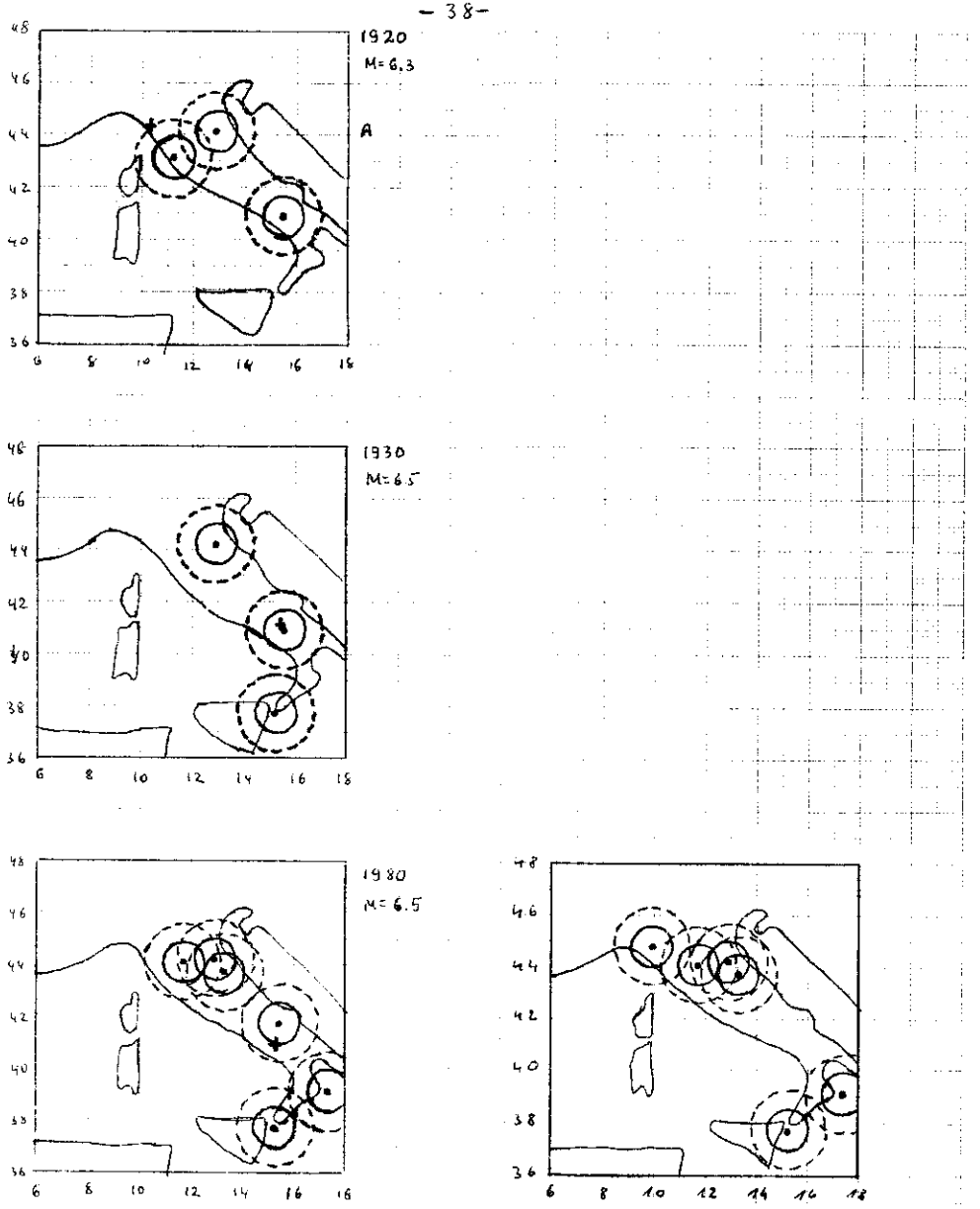

Figure 22. Long range aftershocks in Italy region.

References:

I. Prozorov A.G., Sabina F.J. Study of the properties of seismicity in the Mexico region, Geophys.J.R.astr.Soc. (in print).

2. Prozorov A.G., Dziewonski A.M. A method of studying variations in the clustering property of earthquakes : application to the analysis of global seismicity. J.G.R., v. 87, No B4, pp. 2829-2839, (1982).

3. Prozorov A.G., Rantsman Ye. Ya. Earthquake statistics and the morphostructures of eastern Soviet Central Asia. Doklady Akad.Nauk SSSR, v. 207, No 2, pp. 341-344 (1971).

4. Mogi K. Earthquakes and fractures. Tectonophysics, v.4, No. I, (1967).

5. Myachkin V.I., Kostrov B.V., Sobolev G.A., Shamina O.G. Experimental and theoretical investigations of processes that are possible forerunners of earthquakes. Izv. Akad. Nauk SSSR, Fiz. Zem., 10, pp. 676-679, (1974).

6. Nur A. Dilatancy, pore fluids and premonitory variations of t_s/t_p travel times. BSSA, 62, pp. 1217-1222, (1972).

7. Prozorov A.G. Systematic variations of mean travel time residuals in space and time. PAGEOPH, 115, pp. 675-692, (1977).

8. Prozorov A.G., Hudson J.A., Shimshoni M. The behavior of earthquake magnitudes in space and time. Geophys.J.R.astr.Soc., v.73, pp. 1-16, (1983).

9. Prozorov A., Shimshoni M. and Knopoff L. Magnitude studies from ultra-long-period records. Geophys.J.R.astr.Soc., v.48, pp. 407-414,(1977

10. Prozorov A.G. Magnitude distribution of maximal aftershocks. Doklady Akad.Nauk SSSR (in print).

11. Sadovsky M.A. On the natural lumpishness of the rock samples. Doklady Akad.Nauk SSSR, v. 247, pp. 829-833, (1979).

12. Sadovsky M.A., Bolkhovitinov L.G., Pisar enko V.F. On the property of diskretness of rock samples. Proc.of the Earth Physics Inst., Moscow, (1981)

13. Prozorov A.G. On the low probabilities of the strong shocks in some space-time vicinities of major earthquakes of the world. Computational Seismology, v.11, pp.35-47, (1978).

14. Duda S.J. Secular seismic energy release in the circum-Pacific belt, Tectonophysics, v.2, No. 5, pp.409-452, (1965).

15. Gutenberg B. and Richter C.F. Seismicity of the Earth and associated phenomena, Princeton Univ.Press, 1954.

16. Keilis-Borok V.I., Rotwain I.M., Sidorenko T.V. Increased flow of aftershocks as a forerunner of strong earthquake. Doklady Akad.Nauk SSSR, v. 242,No 3, pp. 567-569, (1978).

17. Keilis-Borok V.I., Malinovskaya L.N. One regularity in the ocurrence of strong earthquakes. J.G.R., v.69, pp. 3019-3024, (1964).

18. Fedotov S.A. Regularity in strong earthquake distribution in Kamchatka, Kuril Islands and North-East Japan. Proc. of the Earth Physics Inst. Moscow, 36, pp. 66-93, (1965).

19. Mogi K. Some features of recent seismic activity in and near Japan. Bull.Earthquake res.Inst.,Univ.Tokyo, 46, pt.6,pp.1225-1236,(1968).

20. Sykes L. Aftershock zones of great earthquakes, seismicity gaps and earthquake prediction for Alaska and Aleutians. J.G.R., v.76, No.32,pp. 8021-8041, (1971).

21. Prozorov A.G. Seismic activity changes related to the strong earthquakes. Computational Seismology, v.8, pp. 71-82, (1975).

22. Prozorov A.G. Long range aftershocks as indicators of strong earthquakes in South California. Computational Seismology, v. 14, pp.20-26, (1982).